IOP Publishing Journal of Optics
J. Opt. 19 (2017) 084005 (16pp) https://doi.org/10.1088/2040-8986/aa7288

Metamaterials in microwaves, optics, mechanics, thermodynamics, and transport

Thomas Koschny[1,4], **Costas M Soukoulis**[1,2] **and Martin Wegener**[3]

[1] Ames Laboratory and Department of Physics and Astronomy, Iowa State University, Ames, IA 50011, United States of America
[2] Institute of Electronic Structure and Laser, FORTH, 71110 Heraklion, Crete, Greece
[3] Institute of Applied Physics and Institute of Nanotechnology, Karlsruhe Institute of Technology (KIT), D-76128 Karlsruhe, Germany

E-mail: koschny@ameslab.gov

Received 27 August 2016, revised 24 April 2017
Accepted for publication 11 May 2017
Published 21 July 2017

Invited Contribution to the Special Issue 'The History of Metamaterials'.

Abstract

We review the status of metamaterials on the occasion of the 15th birthday of the field with particular emphasis on our own contributions. Metamaterials in electromagnetism, mechanics, thermodynamics, and transport are covered. We emphasize that 3D printing, also known as additive manufacturing, inspires metamaterials—and vice versa.

Keywords: metamaterials, photonics, plasmonics, 3D printing

(Some figures may appear in colour only in the online journal)

Introduction

The fundamental idea of metamaterials is that by imposing specific, functional and purposefully designed spatial distributions of just a few, ordinary constituent materials on sufficiently small length scales, we can create new, artificial materials, which as a bulk or effective medium show macroscopic material properties not found in their constituent materials—or not even in any naturally occurring material.

Using just two constituent materials **A** and **B**, one can in many cases achieve effective properties that are *not* in between those of **A** and **B**. The resulting properties can rather be quantitatively and qualitatively different. Sometimes, material **B** can even be a void, i.e., vacuum or air. In this case, one can completely change the effective material properties by making a piece of bulk material **A** porous in a special way. In other cases, more constituent materials **A**, **B**, **C**, … are necessary. In some cases, one can even reverse the sign of some material parameter, in others the effective parameters are unbounded and can, in principle, assume any value from minus infinity to plus infinity for ingredients with some finite value.

It should be noted though that the idea of rationally designed tailored artificial materials or composites is not new. It is at least a century old. Yet, only after the notion 'metamaterial' was coined, corresponding research has been widely perceived as a field on its own. It is instructive to recall some examples (list is not complete), including electromagnetism, mechanics, thermodynamics, and transport:

- Late 1800s: James C Maxwell, microwave laminates with anisotropic behavior from isotropic constituents.
- 1898: Jagadish C Bose, chiral artificial microwave materials from achiral dielectric constituents.
- 1920: Karl Lindman, three-dimensional (3D) chiral artificial microwave materials from achiral metallic constituents. He used helices, which can be seen as stretched-out split-ring resonators (SRRs).
- 1987: Roderic S Lakes, foams with negative Poisson's ratio from positive constituents.
- 1995: Graeme W Milton and Andrej V Cherkaev, pentamode composites enable conceptually synthesizing any elasticity tensor.
- 1996: Roderic S Lakes, composites with any thermal-expansion coefficient from two ordinary constituents and voids.

[4] Author to whom any correspondence should be addressed.

- 1999: Sir John B Pendry, SRR as a simple magnetic resonant sub-wavelength sized structure that enabled practical implementation of metamaterials with strong positive or negative magnetic response.
- 2000: David R Smith, microwave metamaterials with negative refractive index from positive constituents.
- 2009: Marc Briane and Graeme W Milton, sign-reversal of Hall-effect in special 3D chainmail-like micro-lattices.

On this basis, we should humbly admit that a big portion of today's work is about refining known theoretical concepts or about applying them to experiments. Yet, fabrication of metamaterials does pose an interesting scientific challenge on its own. Combined with the 3D printing idea [1], also known and popularized as additive manufacturing, the metamaterials concept might eventually revolutionize our every-day life like Johannes Gutenberg's 2D printing press did in the 1400s or the personal computer did in the 1900s.

Microwave metamaterials

Microwave metamaterials that implemented effective materials with a negative index of refraction were the early focus in this new field. This was achieved by spatially intercalating arrays of metallic loops with a gap SRR, which functioned as tiny LC resonant circuits providing resonant magnetic dipoles with negative magnetic susceptibility just above their resonance frequency, and grids of thin continuous wires, which provided negative electric susceptibility analog to a bulk metal from their 'diluted' plasma response, both with length scales substantially smaller than the wavelength of microwave radiation. As a historically ignored concept, negative index, with all its exotic consequences for wave propagation such as negative refraction, 'perfect' imaging beyond the diffraction limit and optical anti-matter, initially raised controversy about violation of causality and its compatibility with know physics. In 2003, Foteinopoulou, Economou and Soukoulis performed computer simulations [2] on a properly designed negative-index photonic crystal (PC) to show that causality and relativity are not violated by negative refraction. The same year, Crete, Ames, and Bilkent experimentally demonstrated [3, 4] negative refraction in a properly designed PC in the microwave regime and also demonstrated sub-wavelength resolution of $\lambda/3$. The following year, Ames, Crete, and Bilkent fabricated [5, 6] a left-handed material (LHM) with the highest negative-index transmission peak corresponding to a loss of only 0.3 dB cm^{-1} at a frequency of 4 GHz.

In early publications of negative index transmission peaks, sometimes positive index transmission peaks were misidentified as negative index pass-bands because of interference between the main constituents wire grids and SRR arrays in the electric response function. In 2004, Ames and Crete established that SRR also have a resonant electric response, in addition to their magnetic response [7]. The SRR electric response is cut-wire like and can be demonstrated by closing the gaps of the SRRs, thus destroying the magnetic response. In addition, the studies of the electric response of LHMs introduced a very simple criterion to identify if an experimental transmission peak is left- or right-handed. This criterion was later used experimentally by Bilkent and other groups. The predictions by Ames and Crete were confirmed.

A complicating factor was the various electric and magnetic configurations a SRR can couple to electromagnetic radiation depending on orientation and polarization. In 2004, Ames, Crete, and Bilkent studied both theoretically and experimentally the transmission properties of a lattice of SRRs for different incident polarizations [8]. We found that not only the external magnetic field could couple to the magnetic SRR resonance, but also the external electric field. This happens when the incident electric-field vector is parallel to the gap bearing sides of the SRR and is manifested by a dip in the transmission spectrum. The origin of the transmission dip is a resonance arising from the non-zero average magnetic-dipole moment corresponding to resonant circular electric currents excited by the incident electric field. We note that the excitation of the magnetic moment of the SRR by the electric field is an example of a more general bi-anisotropic response that lifts the independence of electric and magnetic properties of the material. In many cases and especially for 3D metamaterials, a bi-anisotropic response is undesirable and can be avoided by more symmetric designs, e.g., multi-gap SRRs that are inversion symmetric. However, the cross coupling can be an advantage for high-frequency metamaterials, which are typically layered structures, enabling the magnetic resonances to be excited—and detected—by the electric field. This finding triggered much of the research on metamaterials operating at optical frequencies (see below).

Following the success of microwave metamaterials, there was a strong desire to scale up their operating frequency range towards optical frequencies with multitudes of potential applications. As geometrically defined spatial structures, metamaterials should scale in frequency inversely proportional to the spatial size, a fact that experimentally held true from radio frequencies throughout the microwave range to about a few THz. In 2005, Ames, Crete, and Imperial College showed that as one further decreases the size of the SRR, the scaling breaks down and the operation frequency saturates at some value [9]. We will come back to this important point below. The same year, the Ames lab group suggested [10] a new 3D LHM design that gives an isotropic negative index of refraction. This design has not been fabricated yet. In 2006, the Ames lab group introduced new designs [11, 12] that were fabricated and tested at GHz frequencies. These new designs were very useful in fabricating negative-index materials at THz and optical wavelengths and can be easily measured for perpendicular propagation. A simple unifying circuit approach [13] offered clear intuitive as well as quantitative guidance for the design and optimization of negative-index optical metamaterials.

Retrieval of effective parameters

Metamaterials are intended to operate as effective media with well-defined 'averaged' optical parameters such as a homogeneous refractive index and impedance despite their discrete

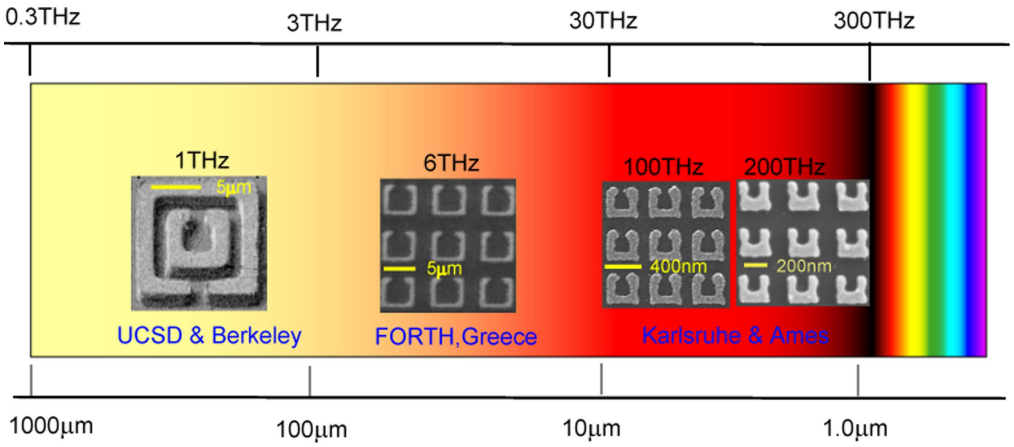

Figure 1. The operation frequency of magnetic metamaterials increased rapidly. The structures operating at 1, 6 and 100 THz frequency, respectively, were fabricated in 2004, and the one at 200 THz in 2005.

constitutive components. It is, therefore, important to have a way to determine these effective parameters from scattering data obtained from either experiments or numerical simulations. In 2002, David Smith and Costas Soukoulis, along with their collaborators, developed [14] a retrieval procedure to obtain the effective electric permittivity ϵ and magnetic permeability μ of electromagnetic metamaterials. They found that the recovered frequency-dependent ϵ and μ are entirely consistent with analytic expressions predicted by effective-medium arguments. Of particular relevance are wire media exhibiting a frequency region in which the real part of ϵ is negative and the SRRs produce a frequency region in which the real part of μ is negative. In the combined structure, at frequencies where both the recovered real parts of ϵ and μ are simultaneously negative, the real part of the index of refraction is also found to be unambiguously negative. This technique is readily applicable to the experimental characterization of metamaterial samples whenever the scattering parameters are known. In 2005, Ames, Crete, and Smith's group introduced [15, 16] a periodic effective-medium theory, which is a significant improvement of the above-mentioned homogeneous effective medium (HEM) approach. This theory explains and resolves all the problems present in the HEM approach (such as the negative product $\mathrm{Im}(\epsilon) \times \mathrm{Im}(\mu)$). The origins of these problems are strong resonances: in some cases, the wavelength inside the metamaterial is comparable to the unit-cell size, and, thus, a homogeneous effective-medium fails to accurately describe the physics.

Optical metamaterials

In the summer of 2004, Costas Soukoulis visited the group of Martin Wegener at KIT. Like the year before, he tried to excite the Wegener group to perform experiments on SRRs approaching optical frequencies. This year, he finally succeeded. A postdoc at KIT, Stefan Linden, went ahead and fabricated planar arrays of gold SRR on glass substrate using standard electron-beam lithography and high-vacuum electron-beam evaporation of gold, followed by a lift-off process. In the optical transmission experiments on very small samples, we took advantage of the fact that, loosely speaking, one can couple to the magnetic-dipole resonance via the magnetic field of the light and via the electric field. The latter can be accomplished under normal incidence of light with respect to the substrate—which was much easier for these early experiments. We varied the lattice constant, opened and closed the slit and thereby unambiguously showed the presence of the predicted magnetic resonance at around 100 THz frequency, equivalent to 3 μm wavelength [17] (compare figure 1). This wavelength was about ten times larger than the side length of the SRR, qualifying the structure as a metamaterial which can be described by effective material parameters.

This result was so exciting because some had expressed skepticism that the magnetic resonance could be scaled to such high frequencies. However, the limit was obviously not yet reached.

In writing that paper, we argued whether or not we should explain our results with a simple model based on an LC resonator. We decided to do so and the simple model became part of the first figure. In retrospect, this was a wise decision because the simple picture built a bridge between the very different languages of microwaves and optics. Many researchers used that picture in their talks afterwards (often without proper citation though).

At this point, an international race started as to which group would be first to further miniaturize and/or modify the SRR to bring its resonance frequency towards the visible—if possible.

In 2005, we published our experimental results on miniaturized gold SRR arrays, which showed a magnetic resonance at twice the frequency, i.e., at around 200 THz, equivalent to 1.5 μm wavelength [18], a band important for communication via optical fibers. By experiments performed under oblique incidence of light, again loosely speaking, we not only coupled to the SRR via the electric field of light, but also via its magnetic field. Only this coupling can be mapped onto an effectively negative magnetic permeability. Clearly, the end of the size scaling was not yet reached.

We also showed that focused-ion-beam milling is an alternative to electron-beam lithography and demonstrated the

transition from square-shaped antennas to SRR as an example [19].

The next year, 2006, we reached the limit of size scaling by further miniaturized SRRs [20] (see above). Having in mind a circuit description, this limit does come somewhat surprising at first sight. After all, the capacitance and the Faraday inductance usually scale inversely proportional to the size of an object upon scaling all of its dimensions by the same factor. Thus, the LC eigenfrequency should also scale inversely proportional to size. It does not though. The reason is the kinetic inductance, which adds to the Faraday induction. At frequencies higher than the damping rate, the electrons in the metal develop a 90 degrees phase lag with respect to the driving electric field of the light. Thus, the metal impedance becomes the sum of the frequency-independent resistance plus the imaginary unit times the frequency times another frequency-independent quantity. This quantity has the unit of an inductance. Just like the usual Ohmic resistance of a wire, it scales inversely proportional to size. Thus, it overwhelms the Faraday inductance at small sizes and leads to a size-independent LC eigenfrequency at very small sizes. Our 2006 work showed that this limit is reached at around 900 nm eigenwavelength—unfortunately just outside of the visible regime.

Fortunately we had seen it coming in 2005 already [21]. Despite of this saturation, the eigenfrequency can be further increased by reducing the capacitance of the SRR. As usual, two identical serial capacitances effectively have half the capacitance, increasing the LC-eigenfrequency by square root of 2. If one additionally opens the capacitive gaps up a bit further, the capacitance decreases even more, further increasing the frequency. In this fashion, one gets a continuous transition between a traditional SRR and a pair of cut wires [21]. Of course, this frequency increase at fixed SRR side length comes with a price: it also means that the ratio of operation wavelength and size of the resonating object decreases significantly, bringing one close to the edge of validity of describing these structures by using effective material parameters. Nevertheless, our optical experiments and the retrieval of effective parameters suggested the possibility of obtaining a negative magnetic permeability—even under normal incidence of light with respect to the substrate.

Such structures were also much simpler to fabricate. For a SRR, the narrow slit has to be fabricated lithographically by methods such as electron-beam lithography. For the cut-wire pair, the slit can be made by evaporating thin films. This simplification enabled large-area structures by parallel interference lithography [22].

By combining these cut wire pairs with long metal stripes parallel to the electric-field vector of the incident light, we arrived at the double-fishnet structure [23], which was previously suggested and investigated by Steven Brueck's group as negative-index metamaterial. Given all the conceptual problems regarding effective-parameter retrieval discussed at that time, we were looking for a smoking-gun experiment. Following the microwave work of David Smith and coworkers, a simultaneously negative electric permittivity and negative magnetic permeability should lead to a negative

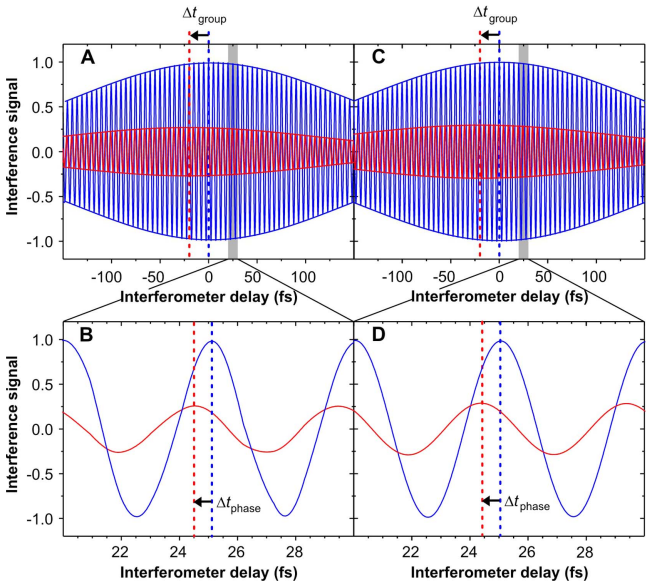

Figure 2. Interferometric experiments on double-fishnet metamaterials operating at telecommunications wavelengths provided smoking-gun evidence for a negative phase velocity of light with respect to the direction of energy flow. However, the group velocity of light can be negative as well. Experiment (left) and theory (right) were in excellent agreement. From [23]. Reprinted with permission from AAAS.

refractive index; or, more precisely, a negative phase velocity of light. Upon propagation of light through such a structure, one should thus observe a negative phase shift as compared to propagation in vacuum. This phase shift should have the spectral signature of the underlying resonances. This phase shift gives direct experimental access to the negative phase velocity of light.

We mention in passing that the situation is less clear in regard to refraction of light at an interface. We have discussed that negative refraction can occur even if all involved refractive indices are positive [24]. This can happen for PCs or at the interface between two birefringent Quartz crystals.

At that time, many researchers showed in their talks movies of simulated pulses propagating through a medium with negative refractive index. They pointed out that the pulse envelope moves say to the right-hand side whereas the underlying carrier wave moves towards the left-hand side. In our experiment using femtosecond pulses, we could not only monitor the carrier wave but also the envelope of the pulse, providing us with information on the group velocity as well (see figure 2). We found a much richer behavior: depending on the pulse center frequency with respect to the magnetic resonance, phase velocity and group velocity could independently be positive or negative, demonstrating four different possibilities. Negative or positive with respect to what? With respect to the Poynting vector of light, which was always positive in our experiments—otherwise, no electromagnetic energy would ever have arrived at our detector [23].

We also investigated the optical properties of these double-fishnet optical metamaterials under oblique incidence of light and for different polarizations [25]. We found an angular dispersion which can be interpreted in terms of spatial

dispersion due to interaction among the different unit cells. We shall come back to effects of interaction in some more detail below.

These structures operating at around 1.5 μm wavelength were based on gold as metal [8]. Soon thereafter, we could reproduce the same effects at comparable wavelength at much lower damping by using silver instead of gold [26].

Stacking three functional layers instead of using just one led to comparable qualitative results, yet to slight frequency shifts due to interaction among the different unit cells [27]. Most importantly, however, the negative phase shifts remained. One year later, Xiang Zhang's group demonstrated ten functional layers.

Using silver and further miniaturizing the dimensions of the double-fishnet structures also allowed us to shift negative phase velocities to 780 nm—a wavelength that is easily visible with the naked human eye [28]. The influence of the design parameters on effective losses was discussed in detail [29].

We also visualized the striking effects of isotropic effective media with negative refractive indices by photo-realistic ray tracing [30].

Let us note in passing that these effects come about due to the fact that dispersion associated with the magnetic resonance is quite pronounced. At first sight, this aspect may appear as an artifact. However, it is intrinsic to negative phase velocities. In the strictly static case, the electric permittivity and the magnetic permeability cannot be negative. Otherwise, one would get an unbounded negative electromagnetic energy density and we would all disappear into oblivion. Thus, in the static case, a negative refractive index is impossible, too. If one aims at a negative refractive index at some frequency, one thus unavoidably needs frequency dependence, i.e., dispersion is intrinsic to negative indices. Causality, i.e., the fact that we cannot change the past can be translated into the Kramers–Kronig relations, which connect the real and imaginary parts of all optical quantities. Thus, it is fundamentally impossible to obtain over an extended frequency regime a negative real part of the refractive index together with zero imaginary part of the refractive index, equivalent to zero absorption.

Our later work on the SRR investigated in more detail the role of retarded SRR interactions [31, 32] and the effects of bi-anisotropy [30]. Both aspects were often ignored in the early phase of the field, but tend to have a significant influence on the optical properties. In particular, bi-anisotropy usually needs to be accounted for when retrieving effective material parameters [33, 34].

Let us be a bit more detailed regarding SRR interactions. It is well known that the long-rang part of the electric-dipole field decays asymptotically inversely proportional to the distance itself. This dependence corresponds to a very long-range interaction. In fact, whatever the finite pre-factor of this term is, the interaction scales like $\propto 1/|N|$, where N is an integer index running from $-\infty$ to $+\infty$ in the simple example of an infinite one-dimensional chain. This sum diverges. It diverges in two and three dimensions as well. At first sight, this finding does not appear to make much sense. The way out is to recall that the interaction is retarded. After all, according to the theory of relativity, no interaction can be instantaneous. For example, consider an array of SRR with a spacing or lattice constant of $\lambda/8$, which is usually considered to be well within the range of the effective-medium approximation. From one SRR to its next-nearest neighbor, the distance is $\lambda/4$, equivalent to a 90 degree phase shift. This means that one SRR does not act on the eigenfrequency of the other SRR but rather acts on the damping. Working out the details leads to an interesting modification of the usual tight-binding picture [32]. For certain parameters, one gets a constant real part of the eigenfrequency but a damping that depends on the wave vector in the plane of the array. This means that the damping one measures in an optical experiment depends on from which angle one looks at the SRR array. One may associate this finding with spatial dispersion. Corresponding experiments have very nicely confirmed this simple qualitative reasoning [32].

By using a modulation approach, we could also measure directly the absolute extinction cross section of individual SRR [35]. Later, we were able to measure scattering and absorption cross-section spectra of SRR separately and quantitatively [36]. By using electron-energy-loss spectroscopy on lithographically fabricated individual SRR, we could measure directly the spatial distribution of the SRR modes [37].

In 2010–2012, we showed in a series of papers that the eigenfrequency of gold SRR can be shifted by as much as 20% by using electrochemical modulation [38–40]. This mechanism works especially well for SRR with a thickness around or below 10 nm, for which the change in electron density in the upmost atomic layer substantially influences the overall electron density within the SRR.

Nonlinear optical metamaterials

In addition to their linear optical properties, Sir John B Pendry also predicted interesting nonlinear optical properties. We thus studied experimentally second-harmonic generation (SHG) from gold SRR arrays under normal incidence of light [41]. We found that the magnetic resonance led to much larger SHG signals than any of the other resonances. Third-harmonic generation was investigated, too [42]. Later, however, we repeated these experiments with complementary SRR instead of SRR and found that the complementary structures yielded comparable SHG signals [43]. Following the generalized Babinet's principle, going from SRR to complementary SRR interchanges the role of magnetic and electric dipoles. Thus, our experiments suggested that the large SHG signals were not really a result of the magnetic resonance but rather a result of the special shape of the SRR.

Later, we investigated the role of SRR interactions on the SHG signals [44] and found that the maximum SHG signal does not occur at the densest packing of SRR—as one might expect intuitively. These results confirmed our earlier work on the effects of SRR interaction on the linear optical properties, which we have already mentioned above.

Along the same lines, also THz radiation can be generated rather efficiently from SRR arrays via difference frequency generation or optical rectification using incident near-infrared light [45]. Efficient single-cycle broadband THz radiation was generated (ranging from about 0.1–4 THz) from a single layer of 40 nm thick metallic SRRs pumped at the telecommunication wavelength of 1.5 μm. This thin metamaterial THz emitter performed as well as traditional emitters (ZnTe) that are more than thousand times thicker (0.2 or 1 mm). The terahertz emission originates from exciting the magnetic dipole resonance of the SRR. Tuning the size of the SRR allowed tuning to a particular pump wavelength; the broad bandwidth of the THz emission is achieved by the bandwidth of the SRR resonance and the short duration of the pump pulse. The experimental results were in good overall agreement with numerical solutions of the Maxwell–Vlasov (or cold-plasma) equations. In essence, these equations are a straightforward generalization of the Drude free-electron model of a metal [43, 45]. The nonlinearities therein arise from the convective term (in analogy to hydromechanics), the Lorentz force, and a surface contribution. The comparison to theory [45] showed a giant sheet nonlinear susceptibility of about $10^{-16}\,\mathrm{m^2\,V^{-1}}$ that far exceeds known thin films and bulk inorganic materials such as ZnTe. Our approach provided a potential solution to bridge the 'THz technology gap'.

The resonant local-field effects of SRRs can also enhance the effective nonlinearities of a material, such as the semiconductor GaAs, which is brought to the near-field of the SRR [46]. Here, the polarization selection rules are distinct from those of SRR arrays on glass substrates, which allowed us for unambiguous identification of this contribution.

Optical metamaterials containing gain media

However, the damping of the SRR resonances has been a nuisance from the start. On or near the SRR resonance, only a few layers of SRR completely block the light, rendering the resulting structures essentially useless. Our experimental efforts [47, 48] to bring gain media into close proximity of SRR arrays operating around 1.5 μm wavelength to compensate for these losses were motivated by our own early theoretical work suggesting this approach might work [49, 50]. However, our efforts over several years based on using thin semiconductor films as gain media in the near field of the SRR were not successful. The experiments did show some loss reduction [47], with line shapes in agreement with theory, but the beneficial effects were not large enough at the end of the day. Thus, we eventually gave up working in this direction.

Nevertheless, we studied loss compensation of SRR structures with a gain layer underneath in quite some detail theoretically. Numerical results showed that the gain layer can compensate the losses of the SRR [51], for light propagating parallel and perpendicular to the plane of the metamaterial layer. Three different gain pumping schemes were applied in the simulations and the efficiencies of their corresponding loss compensations were studied by investigating the linewidth of the resonant current. The homogeneously pumped isotropic gain could significantly reduce the magnetic losses, though it is less efficient in the loss compensation compared to the case with the gain in the SRR gap. The other two schemes, (1) a homogeneously pumped isotropic gain with a shadow cast by the SRR and (2) anisotropic gain only coupled the electric field component parallel to the gap bearing side of the SRR, are much less efficient in the loss compensation compared to the isotropic gain case, due to no interactions between the electric field perpendicular to the SRR plane, E_z, and the gain in these two schemes. We have also studied the effect of the background dielectric of gain. In a very narrow gain layer, the gain dielectric background mainly affects the electric field perpendicular to the GaAs-gain interface due to the continuity of the normal component of the electric displacement across the interface. So, the dielectric background of gain does not make much difference for the gain pumped in the parallel direction only.

We proposed and numerically solved a self-consistent model incorporating gain in the 3D fishnet dispersive metamaterial [52]. We showed numerically that one can compensate the losses of the fishnet metamaterial. We have presented results for the optical transmission T, reflection R, and absorbance A without and with gain for different pump rates. Once the pump rate increases, both T and R show a resonance behavior. We retrieved the effective parameters for different pump rates and the losses were compensated by gain. Kramers–Kronig relations of the effective parameter are in excellent agreement with the retrieved results with gain. The figure-of-merit with gain increased dramatically and the pump rate needed to compensate the loss is much smaller than the bulk gain. This aspect is due to the strong local-field enhancement inside the fishnet structure.

A self-consistent model incorporating the gain into a dispersive metamaterial nanostructure was proposed and numerically solved [53]. We numerically show that the losses of dispersive metamaterials can be compensated by gain by investigating the transmission, reflection and absorption data as well as the retrieved effective parameters. There is a relatively wide range of input signal amplitudes where the metamaterial gain system behaves linearly. When the amplitudes get higher, the system becomes nonlinear, due to the nonlinearity of the gain material itself. It is necessary to have self-consistent calculations to determine the signal range where we can expect a linear response. Further, if we have strong signals, so that we are in nonlinear regime, or we want to study lasing, self-consistent calculation is needed. As examples, two SRR systems with different gain inclusions were studied. We have demonstrated that the magnetic losses of the SRRs can be easily compensated by the electric gain. The pumping rate needed to compensate the losses is much smaller than the bulk gain material. The losses of the SRR surrounded by gain can more easily be compensated than the SRR with gain in the gap, due to more coupling with the gain. Provided that the pumping rate is high enough, metamaterial nanostructures can lase.

We have introduced a new approach for pump-probe simulations of metallic metamaterials coupled to gain materials [54]. We study the coupling between the U-shaped

SRRs and the gain material described by a four-level gain model. Using pump-probe simulations, we find a distinct behavior for the differential transmittance $\Delta T/T$ of the probe pulse with and without SRRs in both magnitude and sign (negative, unexpected, and/or positive). Our new approach verified that the coupling between the metamaterial resonance and the gain medium is dominated by near-field interactions. Our model can be used to design new pump-probe experiments to compensate for the losses of metamaterials.

We mention in passing that we have also demonstrated how the lasing threshold of a two-dimensional (2D) PC containing a four-level gain medium is modified, as a result of the interplay between the group velocity and the modal reflectivity at the interface between the cavity and the exterior [55, 56]. Depending on their relative strength and the optical density of states, we showed how the lasing threshold may be dramatically altered inside a band or, most importantly, close to the band edge. The idea is realized via self-consistent calculations based on a finite-difference time-domain method. The simulations were in good agreement with theoretical predictions.

Graphene for THz applications

Graphene—a one-atom-thick continuous sheet of carbon atoms—has special properties (e.g., electric and chemical tunability, high kinetic inductivity allowing for strongly confined plasmons, large THz optical conductivity) that make it a desirable material for manipulating terahertz waves. THz applications operate at frequencies between microwave and far infrared. Some metamaterials could benefit by replacing the metals currently used in fabrication with graphene. Indeed, graphene provides a number of advantages over metals including that its properties offer the unprecedented ability to tune and/or temporally modulate the electrical response for a given application. Graphene also offers the advantage of a potential enhancement of terahertz wave confinement [57] and smaller, more sub-wavelength metamaterial resonators made from graphene rather than metals. However, as we pointed out in our analysis of published experimental measurements of the THz optical conductivity of graphene [57], the experimental data have shown significantly higher electrical losses at THz frequencies than have been estimated by theoretical work or have been assumed in mostly very optimistic numerical simulations, showing that more research needs to be done to make metamaterial devices from graphene. We also published an analysis and comparison of gold- and graphene-based resonator nanostructures for THz metamaterials and an ultrathin graphene-based modulator [57, 58]. Metamaterial resonators and plasmonic applications have different requirements for what can be considered a good conductor. We published a systematic comparison of graphene, superconductors, and metals as conducting elements in either metamaterials or plasmonics [59].

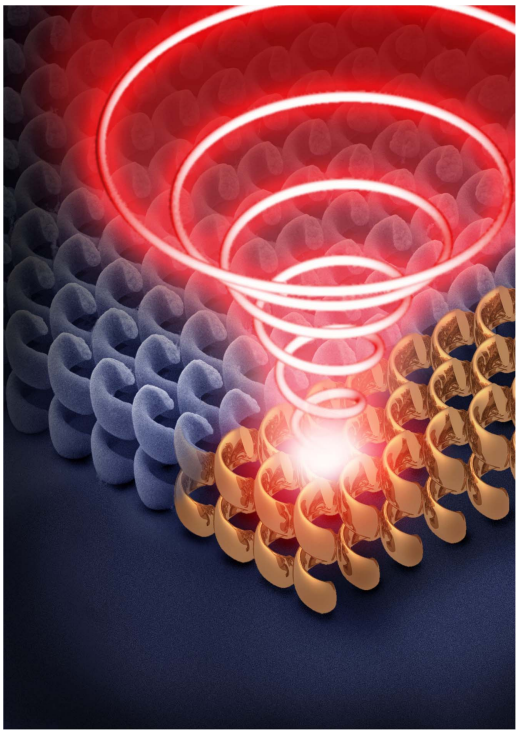

Figure 3. Helical metamaterial made by 3D laser lithography and gold electroplating can be used as broadband circular polarizers. Here, the lattice constant is 2 μm. From [63]. Reprinted with permission from AAAS.

Chiral optical metamaterials

At some point we thus asked ourselves: are magnetic resonances at optical frequencies good for anything? At this point we reminded ourselves that optical activity and circular dichroism can be explained by using magnetic-dipole resonances excited by the electric-field of the light and vice versa. This fact is related to the bi-anisotropy already briefly mentioned above.

Our early work in this direction used SRR or variations thereof arranged into single or different layers [60–62]. These samples were fabricated by using electron-beam lithography of several aligned layers. This led to very large circular birefringence effects at negligible linear birefringence [62]. Experiments and theory were in good agreement.

Helical optical metamaterials

However, the effects become even more pronounced if one makes the transition from a planar SRR to a 3D metallic helix [63] (see figure 3). One can imagine to pick up one end of the wire making up a planar SRR and to pull it out of the SRR plane up into the third direction. This thought experiment suggests that the electromagnetic modes can be transferred adiabatically. For a single winding of the resulting helix, the chiral effects still exhibit a resonant behavior though. Things change substantially for two or more axial pitches of the metal helix. Due to the strong interaction between adjacent pitches

(also see above), the modes hybridize and a broad stop band develops out of the formerly discrete resonances. This means that both Mie and Bragg resonances are beneficial at this point. This chiral stop band can have a width of one octave and means that unpolarized incident light propagating along the helix' axis turns into circularly polarized light. In other words: the array of helices acts as a broadband circular polarizer and forms the analog of the good old linear metal wire-grid polarizer. The same behavior cannot be obtained with a linear polarizer and a quarter-wave plate because an ordinary quarter-wave plate changes into a half-wave plate when changing the wavelength by one octave, i.e., by a factor of two. When using wavelengths of a few micrometers, the high-transmitting polarization can have a transmittance as large as 90%, whereas the low-transmitting state can be as low as just a few %.

More detailed parameter studies showed that the interaction between adjacent helices in an array also significantly influences the extinction ratio and the operation bandwidth [64].

Quite like the SRR, the operation wavelength of the helix scales proportional to the diameter of the helix and is fairly independent on the axial pitch over a large parameter range. This means that one can taper the helix radius along the helix axis and thereby further increase the operation bandwidth to nearly a factor of three in frequency or wavelength [65]. All of these helical structures can be fabricated by using a combination of 3D printing and subsequent gold infilling via electroplating.

A more detailed analysis revealed that the purity of the emerging circular polarization is limited to about 1% though. The reason for this limitation lies in the fact that the wire making up the finite-length helix has an end. This end breaks the symmetry and unavoidably introduces a linear birefringence in addition to the wanted circular birefringence. Our theoretical work showed that symmetry can be recovered by considering three or four intertwined helices arranged onto a periodic lattice such that the lattice has the same symmetry as one of its building blocks [66, 67]. However, the fabrication of such structures posed a significant experimental challenge. After some years of work, we solved this challenge by using 3D laser printing enhanced by stimulated-emission depletion (STED) [68]—the same trick that Stefan Hell got the Chemistry Nobel Prize for in optical microscopy. Our experiments on gold triple helices indeed showed that linear birefringence could be eliminated [69, 70].

Another interesting optical function is to convert left- into right-handed circular polarization. This function can be accomplished by combined left- and right-handed helices over a broad bandwidth [71].

Transformation optics

In 2006, Ulf Leonhard and a team around John B Pendry independently published their famous papers on what is now known as transformation optics and invisibility cloaking. Later, it became clear that precursors for transformation optics and cloaking do exist.

Broadly speaking, transformation optics can be seen as a design tool allowing for mapping intuitive spatial coordinate transformations onto actual material distributions. While one can use that tool for the design of many different structures or devices, one possibility immediately struck the imagination of many, namely that of invisibility cloaking. The mentioned mapping generally leads to spatially inhomogeneous and anisotropic material distributions. Locally, one needs anisotropic materials with large anisotropy. For the example of a cloak, one does not want polarization dependence (birefringence) though. In optics, obtaining anisotropy without birefringence requires that the electric permittivity tensor equals the magnetic permeability tensor everywhere, i.e., one unavoidably needs magnetic properties. Following what we have said above, these are available in principle. However, the losses coming along make actual realizations very difficult if not impossible. In fact, in optics, to the best of our knowledge, no corresponding cloaking experiment has been published to date. An early demonstration of cloaking at microwaves using SRR was published by a team around David Smith in 2006 already.

Conformal transformations (or conformal maps) form a subclass of general spatial transformations. They preserve local angles, which means that, starting from an isotropic medium, one always obtains locally isotropic material properties. In this case, polarization dependence is absent anyway and one does not need magnetism at optical frequencies within the structure. One does still need it at a possible interface to the surrounding medium to obtain impedance matching there. This aspect, however, can sometimes be neglected approximately. In fact, the mentioned 2006 publication by Ulf Leonhard already used conformal mappings. In 2008, Jensen Li and Sir John B Pendry published their paper on the so-called carpet cloak, which was introduced as a quasi-conformal mapping. Later, we showed theoretically that one can also use truncated conformal maps [72] to obtain comparable results in a much simpler manner. Even analytical expressions for the refractive-index profile can be obtained [72].

In a series of papers, we visualized and quantified the performance of various types of invisibility cloaks by using advanced photorealistic ray tracing [73–76].

Experimentally, we published a 3D version of the carpet cloak in 2010 and showed that it works amazingly well from all viewing directions and polarizations in three dimensions. It also works over a broad frequency range. We explicitly demonstrated nearly one octave in bandwidth [77]. The necessary graded-index distribution was realized by a 3D polymeric woodpile PC made by 3D printing and used in the long-wavelength or effective-medium limit. By adjusting the local volume filling fraction of the polymer, the local refractive index could be adjusted. This simple approach was verified by photonic band-structure calculations.

These early structures worked from about 1.5 to 3.0 μm wavelength. By miniaturizing all dimensions, we were later able to shift the operation wavelength down by a factor two,

reaching the red part of the visible range. Again, the above mentioned STED laser lithography was essential [78]. Now, we could see the cloak in action under an optical microscope with our own eyes [78]. By using interferometric imaging, we also showed that the same cloak not only properly recovered the amplitude but also the phase of the light wave quite well [79].

While some initially dreamt about making soldiers or other macroscopic objects invisible with respect to the surrounding air, it is now clear that accomplishing this dream is fundamentally impossible—at least for a broad range of frequencies and for all directions in free space. After all, the light must make a detour around the object to be hidden. To compensate for this geometrical detour, the light has to speed up with respect to the surrounding to arrive on the downstream side of the cloak after the same time or same optical path length as if nothing was there. Speeding up with respect to air or vacuum corresponds to superluminal propagation. The phase velocity of light can exceed the vacuum speed of light. However, for broadband operation, dispersion must be negligible. In this case, the energy velocity equals the phase velocity. According to Albert Einstein's theory of relativity, superluminal energy or mass transport is not possible. In other words, a macroscopic electromagnetic cloak that works for all directions in vacuum or air must inherently be dispersive.

It is sometimes said that an electromagnetic cloak at one frequency is equivalent to electromagnetic vacuum. If that was true, a relativistically moving invisibility cloak should appear as relativistically moving vacuum, i.e., just as vacuum. In 2016, we showed theoretically that this is not the case [80]. Due to the relativistic Doppler effect, the operation frequency seen from the laboratory frame is shifted when transformed into the co-moving frame. Combined with the discussed unavoidable frequency dependence of the cloak, this means that the light sees the wrong material-parameter distribution within the cloak. The Doppler shift can be pre-compensated for infinitely many special conditions, but cloaking becomes non-reciprocal for these conditions [80].

The trick for the above carpet cloak is that the surrounding medium is not air but rather a dielectric with a refractive index larger than unity. Due to the gentle conformal map, the phase velocity of light exceeds the vacuum speed of light at no point within the cloak. Thus, broadband operation is allowed. However, the carpet cloak forbids inspection of the structure from one half-space by construction—it is not a free-space cloak. One can 'glue' two carpet cloaks back to back though and obtain a free-space cloak for one direction [81].

If one ignores phase shifts, all of the above fundamental restrictions no longer apply. For example, one can ignore phase shifts for the case of cloaked metal contacts on solar cells [81]. For most commercial solar cells today, metal contacts on the Sun-facing side are required electrically, but not wanted optically because they shadow part of the area and thereby effectively reduce the solar cell energy conversion efficiency. Mapping a spatial transformation onto the local inclination angle of the surface of a dielectric on top of the solar cell leads to a special free-form surface. This free-form surface refracts light such that it does not hit the metal contact. For normal incidence, light is rather evenly distributed across the remaining area. The structure still works for oblique incidence of light. For metal filling fractions as large as 20%, we even showed that such cloak is ideal. This means that no light ray ever hits the metal contact, regardless of color, angle, or polarization. If the solar cell fully absorbs the light, as it should, one no longer sees any contacts when looking at the solar cell. In fact, the structure just appears homogeneously black. Possibly, this geometry turns into an actual application of optical invisibility cloaking. The mentioned cloaks can also be mass fabricated by using stamping replication techniques [81]. However, one should be clear that the shadowing metal contacts are only one aspect of a complete solar cell. Its overall optimization is a more involved story on its own.

Cloaking for diffuse light

Our above considerations regarding the impossibility of certain classes of cloaks were not meant as a negative statement. These considerations rather inspired us to consider various other types of cloaks that are possible. The above arguments collapse if one considers instead vacuum or air as surrounding dielectrics with an off-resonant refractive index of, say $n = 100$ or even 1000. Therein, light of any color is slowed down so much that one has plenty of room to go up before reaching the fundamental limit of the vacuum speed of light. However, such dielectrics are not known to mankind—at least not at optical frequencies.

This also points to the fact that any cloak is only a cloak with respect to a specific surrounding. For example, an ideal optical invisibility cloak for one color in vacuum or air will appear as a void if exposed to water with a refractive index around $n = 1.33$. It will also appear as a visible void if the same invisibility cloak enters a cloud, fog or some other turbid light-scattering medium.

Turbid media effectively slow down the propagation of light due to multiple scattering events, which lead to a distributed detour. The slowing down can easily reach factors as large as 100 or 1000. However, in a scattering medium, one no longer has a unique speed but rather a statistical distribution. On this basis, macroscopic invisibility cloaks become possible that work for all directions, colors and polarizations of incident visible light. This is true for cloaks designed via coordinate transformations but also approximately true for simplified core–shell cloaks. One can think of the latter as just one period of a laminate metamaterial composed of one layer (the core) with low diffusivity for light and a second layer (the shell) with high diffusivity. This geometry can even be exact under stationary conditions and for constant gradients across the structure, i.e., for homogeneous illumination conditions. This fact was already shown by Kerner in 1956. His abstract speaks about 'coated grains' and the paper deals with 'neutral inclusions' as a special case.

In our first set of experiments [82] based on water mixed with white wall paint as the surrounding, we aimed at

experiments being well within the diffusive regime. We showed that cloaking does work well for cylindrical as well as for spherical core–shell geometry throughout the entire visible spectrum. Amazingly, the simplified core–shell approach also worked very well under highly inhomogeneous illumination and even for illumination conditions breaking the symmetry of the setting.

Using the same samples, we later showed that these diffuse-light cloaks can be revealed under pulsed excitation and time-resolved imaging [83]. The timescales, however, must be shorter than the diffusion time. Under our conditions, the diffusion time was around a few nanoseconds. These timescales are so short because the vacuum speed of light is so large. Mathematically, this failure arises from the fact that the time-dependent diffusion equation is not form invariant under general coordinate transformation. This form invariance is an important necessary condition for the mentioned mapping of coordinate transformations onto material parameters to work. Plainly speaking, the diffusion equation contains only one material parameter, namely the diffusivity, whereas mathematically one would need at least two parameters. Intuitively, the cloaking shell has a larger diffusivity for light than the surrounding to compensate for the near-zero diffusivity of the core. The larger diffusivity of the shell also means that the diffusion time, which is inversely proportional to the diffusivity, is shorter for the shell than for the surrounding. Indeed, our experiments and calculations showed that light emerged faster from the cloak than from the reference structure [83]. Thus, the region behind the obstacle appeared too bright with respect to the reference at early times and too dark at late times. This finding can be applied in terms of high-end security features [83]: a hidden code is invisible under ordinary illumination conditions and can be read-out with high contrast under pulsed illumination.

Our second generation of samples was all solid state [84]. It was based on polydimethylsiloxan (PDMS) doped with titania nanoparticles and a ceramic core with low absorption. All observations of the first generation could be reproduced. However, due to a much lower concentration of scattering centers, the optical transmittance was about an order of magnitude higher than in the first generation of samples and reached nearly 10%. Due to the lower absorption from the core, the cloaking performance was even better than in the first generation of samples. The lower concentration of scattering particles stresses the validity of the diffusion equation though. We later showed by extensive Monte-Carlo ray-tracing calculations that this approach can span the bridge from the ballistic to the diffusive regime, leading to yet better agreement between experiment and theory [85].

Monte-Carlo ray-tracing was crucial to design structures aiming at making metal contacts on large-area organic light-emitting diodes invisible in the sense of homogenizing the light emission. Here, light transmittance is obviously of utmost importance. Within the diffusion equation, the transmittance cannot be larger than 50% because forward and backward scattering must be equally probable within the diffusive regime. We discussed different options and showed one simple solution based on piece-wise homogeneous and isotropic triangular regions on top of the metal contact. Again, experiment and theory were in very good agreement [86].

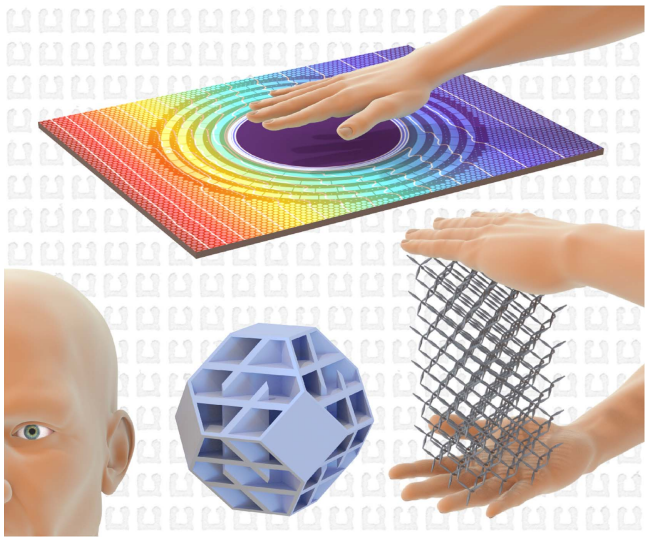

Figure 4. The concept of metamaterials is not restricted to electromagnetism or optics, but can also be applied to many other areas, such as thermodynamics, acoustics, and mechanics. From [106]. Reprinted with permission from AAAS.

Cloaking for heat conduction

Historically, these light-diffusion experiments were actually triggered by our earlier experiments on cloaking in heat conduction. Mathematically, heat conduction and diffusion are rather similar. Both describe the increase of entropy. There is a subtlety though: the heat-conduction equation contains two parameters, namely the heat conductivity and the specific heat, whereas the diffusion equation contains only one parameter (see above). Thus, even the time-dependent equation is strictly form-invariant under arbitrary coordinate transformations.

In these earlier experiments [87] (see figure 4), which were suggested to us by Sebastien Guenneau and performed in collaboration with him, we used multiple shells rather than just a single shell. The structures were designed by a coordinate transformation mapped onto a binary metamaterial distribution composed of high-conductivity copper and low-conductivity PDMS. Alternating concentric rings led to the necessary anisotropy, perforation of the rings to a grading of the anisotropy from the outer to the inner radius of the 2D cloak. By using an infrared camera, we were able to take movies of the transient temperature profiles. We showed that a central area can be protected from heating transiently, while not perturbing the flow of heat in the surrounding of the cloak with respect to a reference structure. We emphasized that the protection only works under transient conditions. If the heat conductivity of the innermost ring is strictly zero over a finite distance, no heat will ever flow into the center. However, if it is very small but finite, heat will eventually flow towards the inside and heat it up [87] (also see supplementary material). In

these experiments, the heat conductivity plays the role of the refractive index in optics. Things work so well in heat conduction because it is easy to obtain a contrast in heat conductivity between copper and PDMS larger than 1000, whereas getting corresponding index contrasts is not possible (see above).

Finally, we mention that cloaking in light diffusion and heat conduction are comparably simple because one effectively deals with a scalar differential equation. Plainly speaking, one simply has no waves in these cases and polarization does not enter. Thus, the effects of scattering, reflection, and interference are absent.

Cloaking in mechanics

In continuum mechanics, one generally and usually has two transverse and one longitudinal polarization of waves. They are often referred to as shear waves and compression waves, respectively. In sharp contrast, one usually has only two transverse polarizations in electromagnetism and optics. In acoustics, only one longitudinal polarization occurs. As a result, the continuum mechanics equations are not form invariant under general curvilinear coordinate transformations —at least not for the elasticity tensors of ordinary materials. In 2006, this result was mathematically proven by Graeme W Milton. This fact means that one cannot generally design cloaks along the same lines as in electromagnetism. Mechanics are more involved than electromagnetism. This may appear somewhat surprising in view of the fact that linear continuum mechanics derive just from Newton's law combined with Hooke's law—two simple laws one learns about in the first semester of physics.

The difficulty regarding the three polarizations can be circumvented in special geometries. Examples are elastic waves in thin plates or membranes, usually referred to as flexural waves. Here, one has only a single essentially transverse polarization normal to the plane of the plate and waves can only propagate in a 2D world. An advantage compared to optics is that a much larger contrast of the elastic Young's modulus (the analog of the inverse of the permittivity in optics) can be obtained under off-resonant conditions. For our choices of the two polymers polyvinylchloride and PDMS, the Young's moduli are different by more than three orders of magnitude. The fabricated structures were closely similar to those discussed for the thermal cloaks discussed above, except that we used a larger number of concentric rings [88]. Importantly, one cannot increase the wave speed of a plate by perforating it. However, near the inner radius of the cloak, one does need wave speeds larger than in the surrounding. Thus, we have lowered the wave speed in the surrounding by perforating the plate. Measurements of wave propagation were performed by launching a Bloch wave via a loudspeaker from one edge of the sample and monitoring the motion of the plate by imaging the plate using an optical camera under diffuse stroboscopic illumination with white light. The experimental results showed good cloaking quality in the frequency range from 200 to 500 Hz. We emphasize once again that the structure does not exploit any resonances.

However, in the more general 3D case, mechanical cloaking cannot be obtained along these lines. We thus got interested in the concept of pentamode mechanical metamaterials. These were suggested theoretically by Andre V Cherkaev and Graeme W Milton in 1995 already. They suggested a lattice composed of double-cone elements, the tips of which touch on a diamond lattice of points with lattice constant a. Intuitively, it is easy to deform or shear the structure while maintaining its volume, whereas it is difficult to change its volume while maintaining its shape. Precisely, the shear modulus is zero while the bulk modulus is finite. This structure can be seen as a solid that acts like a gas or fluid. Our idea was to approximate this ideal by making the connection points small yet finite in volume, with diameter d. Indeed, we could show by numerical calculations that bulk modulus scales as $B \propto d$ and the shear modulus as $G \propto d^3$, leading to a ratio that scales like $B/G \propto 1/d^2$. Moreover, for realistically accessible ratios d/a, ratios as large as $B/G \approx 1000$ appeared to be in reach. We fabricated microscopic [89] and macroscopic [90] versions of such pentamode mechanical metamaterials by 3D printing. The fabricated structures indeed supported ratios as large as $B/G \approx 1000$.

In these structures, the bulk modulus is essentially only determined by the d/a ratio and by the Young's modulus of the constituent material. This means that one can take the thick part of the double-cones to adjust the effective mass density. Our calculations showed that these modified pentamode mechanical metamaterials allow for tailoring pretty much independently the effective bulk modulus and the effective mass density by two geometrical parameters. We were also able to fabricate corresponding structures [91]. These structures might become important for wave experiments, for which phase velocity and wave impedance can be adjusted independently over a fairly large range.

We have also constructed laminates of such modified pentamode mechanical metamaterials [91]. The parameters can be adjusted such that the bulk moduli of the layers are the same, whereas the mass density alternates from one layer to the next. On this basis, we showed that anisotropic mass density tensors can be realized in a fairly intuitive manner [91].

Soon thereafter, we used pentamode mechanical metamaterials to construct a simple core–shell cloak in the static regime [92]. We called it an 'unfeelability cloak', because one would not be able to distinguish reference and cloak by touching the structure. Moreover, the displacements-vector fields outside of the cloak are the same as those of the reference as well. These structures contained more than 1000 3D face-centered-cubic pentamode micro-structured unit cells made by 3D printing.

However, this cloak was limited to small shear moduli. Later, we designed 2D structures based on what we called the direct-lattice-transformation approach [93]. In ordinary transformation optics, a transformation is mapped onto a material-parameter distribution. However, this material-parameter distribution still needs to be mapped onto a concrete

microstructure. At present, no direct way is known to solve this inverse problem. The direct-lattice-transformation approach avoids this difficulty. We start from a specific lattice. As an example, we choose the 2D counterpart of 3D pentamode metamaterials, namely 2D bimode metamaterials. These are composed of a hexagonal lattice of double-trapezoidal elements. Upon performing a coordinate transformation, the positions of the lattice points change accordingly. This implies that the distance between adjacent lattice points and hence the length of the double-trapezoidal elements changes. To obtain the same overall Hooke's spring constant of the structure, we adjusted the width of each individual double-trapezoidal element such that its Hooke's spring constant stays constant. Clearly, this approach ignored shear forces and it also completely ignored what happens to the mass density. In the static case, the mass density drops out. Nevertheless, we obtained excellent cloaking results, both for large B/G ratios as well as for ordinary B/G ratios [93]. Experiments on 3D printed structures and numerical calculations were in excellent agreement. More recently (unpublished), we also showed numerically that cloaking is quite good and broadband in the dynamic wave case.

The possibility of negative effective mass densities at finite frequencies further enhances the possibilities of molding the flow of mechanical waves [94]. By numerical calculations, we showed that corresponding mechanical metamaterials can be 3D printed from just one constituent material [95]. We have also fabricated corresponding micro-lattices by 3D printing. However, the number of lattice cells of these complicated unit cells was rather limited, such that meaningful experiments have not been possible so far.

Reversing the sign of the thermal-expansion coefficient

As pointed out in the introduction, one of the most striking aspects of metamaterials is that the sign of an effective material parameter can be reversed in composites made out of several ingredient materials **A**, **B**, **C** … Regarding the thermal-length expansion coefficient, things are special. Any composite made from some material **A** and air voids (=**B**) within will have exactly the same thermal length-expansion coefficient as **A**—at least within the range of validity of continuum mechanics. However, some years ago, Roderik Lakes already suggested metamaterials composed of two materials **A** and **B** and air voids within that can lead to effectively unbounded behavior. For example, if **A** and **B** have different but positive length-expansion coefficients, the effective length-expansion coefficient of the composite can be negative, minus infinity, plus infinity, or zero. The latter is likely the most technologically relevant case, because uncontrolled thermal length expansion leads to failure or destruction of structures in many every-day-life situations.

The basic idea behind the construction of such metamaterials is to build a 3D lattice composed of bi-material beams. Both materials shall have positive expansion coefficient. Upon temperature increase, the bi-material beams will expand and bend. In a suitable structure, the bending can be translated into a rotation of some structural element, which is then translated into an effective shrinkage of the overall lattice. Along these lines, any effective thermal length-expansion coefficient can be achieved.

Experimentally, the difficulty lies in fabricating a micro-lattice composed of two different ingredient materials and voids within. Most of the structures discussed so far, were composed of only one ingredient material and voids within. We realized two-component structures by using gray-tone optical lithography [96]. Of course, the thermal length-expansion coefficient depends on the type of polymer used. However, we found out that for a given polymer it also depends on the light exposure dose used during fabrication. The exposure dose determines the cross-linking density and hence the material properties. Along these lines, we were able to fabricate the corresponding complex two-component micro-lattices from a single photoresist [96]. To measure the metamaterial properties, we implemented a setup based on cross-correlation analysis of optical microscope images of the samples taken for different temperatures. This allowed us to directly visualizing the displacement-vector fields with a precision much better than a single camera pixel and a precision way below the wavelength of light [96]. This visualization revealed the anticipated sign reversal of the expansion coefficient und confirmed the design mechanism.

Nonlinear buckling mechanical metamaterials

In a 2013 theoretical paper, Graeme W Milton showed that one can obtain any effective mechanical nonlinearity in a metamaterials from purely linearly elastic ingredients. We all wish that something like that was possible in optics. This possibility can be seen as yet another striking possibility of metamaterials. Moreover, one can also obtain multi-stable hysteretic mechanical metamaterials from a single purely linear ingredient with voids within [97]. The starting point is buckling of pre-bent beams, which is well know from textbook mechanics. The physics is similar to the lid of a marmalade jar: upon pushing on the lid, it is first hard corresponding to a large Hooke's spring constant. When pushing further down, the force decreases at some point until it often makes some sort of a 'click'. This regime exhibits a negative differential stiffness. Together, the force versus displacement exhibits an s-shaped behavior. Things get more interesting when considering a sequence of serial nonlinear buckling elements. As for ordinary Hooke's springs, the individual displacements add up to the total displacement and the forces on all elements need to be the same under steady-state conditions. Working out these simple rules led to an amazingly rich behavior [97]. Once one buckling element buckles, all the other ones have to adjust, leading to a non-local interaction. The result is a multi-stable behavior with switching processes and hysteresis. This means that one gets a different force upon loading than upon unloading. Hence, energy is absorbed in one cycle of loading and unloading. This energy absorption mechanism is different from both

usual viscoelastic damping and irreversible destruction of structures like aluminum foams—one of the gold standards of energy absorbers. After completing one cycle, the buckling mechanical metamaterial can be the same, i.e., it is reusable.

We fabricated corresponding polymer samples by 3D laser printing and showed the anticipated energy absorption. The behavior stayed the same after many tens of loading-unloading cycles and depended only weakly on cycling speed [97].

The structures can alternatively be designed to stay in a buckled state such that one needs to actively bring it back to the original state. We have demonstrated experimentally six different programmable states. Around each such state, the linear Hooke' spring constant is different by as much as a factor of five. This means that we could program different spring constants in such a metamaterial.

Reversing the sign of the Hall coefficient

The second example exhibiting a sign reversal of some effective material parameter with respect to its constituents under steady-state conditions is the classical Hall effect. Herein, the magnetic component of the Lorentz force on charged carriers is perpendicular to the imposed electric current and perpendicular to an externally applied static magnetic field. Charges accumulate, and a perpendicular electric field builds up until the total transverse force is zero. The corresponding Hall voltage is inversely proportional to the charge density of the carriers, which can be negative or positive. For example, n-doped bulk silicon results in a negative Hall voltage and p-doped silicon in a positive Hall voltage.

In 2009, Marc Briane and Graeme W Milton showed that the sign of the Hall coefficient can be reversed in 3D chain-mail-like metamaterials. The same is not possible in 2D metamaterials. The Hall coefficient is directly connected with the off-diagonal elements of the conductivity tensor. We note in passing that a sign reversal of the diagonal elements of the conductivity tensor, i.e., the usual electric conductivity, is not possible in passive media due to the second law of thermodynamics.

In 2015, we showed theoretically that such sign reversal can be obtained by using only a single constituent material and air voids within. This means that one can make n-doped silicon porous in a special way and obtain a Hall voltage corresponding to a p-doped material [98]. The corresponding micro-lattices were composed of massive or hollow conductive tori arranged onto a simple-cubic 3D lattice. Depending on whether the tori are sufficiently interlinked or not, we obtained a sign reversal of the Hall resistance or an ordinary behavior. In anisotropic structures, the Hall voltage can also be parallel (rather than orthogonal) to the magnetic-field vector [99].

In 2016, we fabricated Hall-effect metamaterials by 3D printing polymer scaffolds that were subsequently coated with a thin film of n-doped ZnO by using atomic-layer deposition. We obtained Ohmic contacts by shadow evaporation of titanium and gold films. The samples were then exposed to a static magnetic field in a home-built probe station [100]. Upon varying a displacement parameter, we observed the predicted sign reversal of the Hall coefficient. In principle, for a given constituent material, the effective metamaterial Hall resistance can assume any value from minus infinity to plus infinity.

We finally note that the classical (static) Hall effect is nonlinear in that the Hall voltage (or Hall electric field) is proportional to the applied static magnetic field and proportional to the applied static electric field driving the constant electric current. The dynamic version of the classical Hall effect, the photon-drag effect, is a particular second-order nonlinear optical mechanism, which is generally nonzero—even in the presence of centro-symmetry. Here, an incident electromagnetic wave replaces the static magnetic and the static electric field. Thus, one could likewise control the sign and magnitude of particular effective second-order nonlinear optical coefficients by tailored chainmail-like 3D metamaterials.

Conclusion

We have pointed out that many fundamental metamaterial effects have been demonstrated experimentally in microwaves, optics, thermodynamics, mechanics and transport. Most scientifically fascinating to the authors are sign reversals of effective material parameters and the possibility of cloaking in all of these areas. Sign reversal has been shown for the magnetic permeability, refractive index (also see the reviews [101–105]), dynamic mass density, differential mechanical stiffness (also see the reviews [94, 106, 107]), thermal length-expansion coefficient, and the Hall coefficient.

Now that many basic effects have been demonstrated, where are the potential real-world applications? In 2016, a major sports manufacturer brought onto the consumer market 3D printed sports shoes. Their soles contain 3D polymer-based pentamode mechanical metamaterials (see [89–92]), allowing for adjusting the stiffness and the shear forces. Possibly, future soles will even contain tailored anisotropies according to orthopedic requirements.

The connection between metamaterials and 3D printing illustrated by this example may be more far-reaching. Additive manufacturing, a more generic term for 3D printing of materials, is a huge trend worldwide. It allows for fabricating structures that were difficult or even impossible to make previously. Fabricated structures no longer need to be stored. In addition, products can be individualized without additional cost. Multi-billion dollar markets with large growth rates are anticipated. Some foresee that in ten years' time, 10% of all manufactured goods will be 3D printed. Eventually, one would like to 3D print anything, including entire functional devices. Getting there requires an enormous boost regarding spatial printing resolution and printing speed. Moreover, most functional devices require different materials as ingredients; some even require a lot of materials. It is not conceivable that future 3D printers will house hundreds or thousands of different constituent-material

'cartridges'. Today's 2D graphical printers mix thousands of different colors from just three cartridges. By analogy, the metamaterials concept allows obtaining thousands of different effective material properties from just a few constituent-material cartridges. In this sense, the metamaterials concept and 3D printing may be intimately interwoven.

Acknowledgments

MW acknowledges support by the Hector Fellow Academy, the Deutsche Forschungsgemeinschaft (DFG) through DFG-SPP 1839, by the Helmholtz Program *Science and Technology of Nanosystems*, and by the Karlsruhe School of Optics & Photonics (KSOP). Work at Ames Laboratory was partially supported by the US Department of Energy, Office of Basic Energy Science, Division of Materials Sciences and Engineering (Ames Laboratory is operated for the US Department of Energy by Iowa State University under Contract No. DE-AC02-07CH11358), and by the US Office of Naval Research, Award No. N00014-16-1-2294. The European Research Council under ERC Advanced Grant No. 320081 (PHOTOMETA) supported work at FORTH.

References

[1] Deubel M, von Freymann G, Wegener M, Pereira S, Busch K and Soukoulis C M 2004 Direct laser writing of three-dimensional photonic crystal templates for telecommunications *Nat. Mater.* **3** 444
[2] Foteinopoulou S, Economou E N and Soukoulis C M 2003 Refraction at media with negative refractive index *Phys. Rev. Lett.* **90** 107402
[3] Cubukcu E, Aydin K, Ozbay E, Foteinopoulou S and Soukoulis C M 2003 Negative refraction by photonic crystals *Nature* **423** 604
[4] Cubukcu E, Aydin K, Ozbay E, Foteinopoulou S and Soukoulis C M 2003 Subwavelength resolution in 2D photonic crystal-based superlens *Phys. Rev. Lett.* **91** 207401
[5] Aydin K, Guven K, Zhang L, Kafesaki L, Soukoulis C M and Ozbay E 2004 Experimental observation of true left-handed transmission peak in metamaterials *Opt. Lett.* **29** 2623
[6] Koschny T, Kafesaki M, Economou E N and Soukoulis C M 2004 Effective medium theory of left-handed materials *Phys. Rev. Lett.* **93** 107402
[7] Katsarakis N, Koschny T, Kafesaki M, Economou E N and Soukoulis C M 2004 Electric coupling to the magnetic resonance of split ring resonators *Appl. Phys. Lett.* **84** 2943
[8] Katsarakis N, Konstantinidis G, Kostopoulos A, Penciu R S, Gundogdu T F, Kafesaki M, Economou E N, Koschny T and Soukoulis C M 2005 Magnetic response of split-ring resonators in the far infrared frequency regime *Opt. Lett.* **30** 1348
[9] Zhou J, Koschny T, Kafesaki M, Economou E N, Pendry J B and Soukoulis C M 2005 Limit of the negative magnetic response of split-ring resonators at optical frequencies *Phys. Rev. Lett.* **95** 223902
[10] Koschny T, Zhang L and Soukoulis C M 2005 Isotropic three-dimensional left-handed metamaterials *Phys. Rev.* B **71** 121103
[11] Zhou J, Zhang L, Tuttle G, Koschny T and Soukoulis C M 2006 Negative index materials using simple short wire pairs *Phys. Rev.* B **73** 041101
[12] Zhou J, Koschny T, Zhang L, Tuttle G and Soukoulis C M 2006 Experimental demonstration of negative of index of refraction *Appl. Phys. Lett.* **88** 221103
[13] Zhou J, Economou E N, Koschny T and Soukoulis C M 2006 A unifying approach to left handed materials design *Opt. Lett.* **31** 3620
[14] Smith D R, Schultz S, Markos P and Soukoulis C M 2002 Determination of permittivity and permeability of metamaterials from scattering data *Phys. Rev.* B **65** 195104
[15] Koschny T, Markos P, Economou E N, Smith D R, Vier D C and Soukoulis C M 2005 Impact of the inherent periodic structure on the effective medium description of left-handed and related meta-materials *Phys. Rev.* B **71** 245105
[16] Smith D R, Vier D C, Koschny T and Soukoulis C M 2005 Electromagnetic parameter retrieval from inhomogeneous metamaterials *Phys. Rev.* E **71** 121103
[17] Linden A, Enkrich C, Wegener M, Zhou J, Koschny T and Soukoulis C M 2004 Magnetic response of metamaterials at 100 THz *Science* **306** 1351
[18] Enkrich C, Wegener M, Linden S, Burger S, Zschiedrich L, Schmidt F, Zhou J, Koschny T and Soukoulis C M 2005 Magnetic metamaterials at telecommunication and visible frequencies *Phys. Rev. Lett.* **95** 203901
[19] Enkrich C, Pérez-Willard F, Gerthsen D, Zhou J, Soukoulis C M, Wegener M and Linden S 2005 Focused-ion-beam nanofabrication of near-infrared magnetic metamaterials *Adv. Mater.* **17** 2547
[20] Klein M W, Enkrich C, Wegener M, Soukoulis C M and Linden S 2006 Single-slit split-ring resonators at optical frequencies: limits of size scaling *Opt. Lett.* **31** 1259
[21] Dolling G, Enkrich C, Wegener M, Zhou J, Soukoulis C M and Linden S 2005 Cut-wire pairs and plate pairs as magnetic atoms for optical metamaterials *Opt. Lett.* **30** 3198
[22] Feth N, Enkrich C, Wegener M and Linden S 2007 Large-area magnetic metamaterials via compact interference lithography *Opt. Express* **15** 501
[23] Dolling G, Enkrich C, Wegener M, Soukoulis C M and Linden S 2006 Simultaneous negative phase and group velocity of light in a metamaterial *Science* **312** 892
[24] Wegener M, Dolling G and Linden S 2007 Backward waves moving forward *Nat. Mater.* **6** 475
[25] Dolling G, Wegener M, Schädle A, Burger S and Linden S 2006 Observation of magnetization waves in negative-index photonic metamaterials *Appl. Phys. Lett.* **89** 231118
[26] Dolling G, Enkrich C, Wegener M, Soukoulis C M and Linden S 2006 A low-loss negative-index metamaterial at telecommunication wavelengths *Opt. Lett.* **31** 1800
[27] Dolling G, Wegener M and Linden S 2007 Realization of a three-functional-layer negative-index photonic metamaterial *Opt. Lett.* **32** 551
[28] Dolling G, Wegener M, Soukoulis C M and Linden S 2007 Negative-index metamaterial at 780 nm wavelength *Opt. Lett.* **32** 53
[29] Dolling G, Wegener M, Soukoulis C M and Linden S 2007 Design-related losses of double-fishnet negative-index photonic metamaterials *Opt. Express* **15** 11536
[30] Dolling G, Wegener M, Linden S and Hormann C 2006 Photorealistic images of objects in effective negative-index materials *Opt. Express* **14** 1842
[31] Decker M, Burger S, Linden S and Wegener M 2009 Magnetization waves in split-ring-resonator arrays: evidence for retardation effects *Phys. Rev.* B **80** 193102

[32] Decker M, Feth N, Soukoulis C M, Linden S and Wegener M 2011 Retarded long-range interaction in split-ring-resonator square arrays *Phys. Rev.* B **84** 085416
[33] Rill M S, Plet C, Thiel M, Staude I, von Freymann G, Linden S and Wegener M 2008 Photonic metamaterials by direct laser writing and silver chemical vapor deposition *Nat. Mater.* **7** 543
[34] Kriegler C E, Rill M S, Linden S and Wegener M 2010 Bianisotropic photonic metamaterials *IEEE J. Sel. Top. Quantum Electron.* **16** 367
[35] Husnik M, Klein M W, Feth N, König M, Niegemann J, Busch K, Linden S and Wegener M 2008 Absolute extinction cross section of individual magnetic split-ring resonators *Nat. Photon.* **2** 614
[36] Husnik M, Linden S, Diehl R, Niegemann J, Busch K and Wegener M 2012 Quantitative experimental determination of scattering and absorption cross-section spectra of individual optical metallic nanoantennas *Phys. Rev. Lett.* **109** 233902
[37] Boudarham G, Feth N, Myroshnychenko V, Linden S, Stephan O, Colliex C, Garcia de Abajo J, Wegener M and Kociak M 2010 Spectral imaging of individual split-ring resonators *Phys. Rev. Lett.* **105** 255501
[38] Shao L, Ruther M, Linden S, Essig S, Busch K, Weissmüller J and Wegener M 2010 Electrochemical modulation of photonic metamaterials *Adv. Mater.* **22** 5173
[39] Ruther M, Shao L, Linden S, Weissmüller J and Wegener M 2011 Electrochemical restructuring of plasmonic metamaterials *Appl. Phys. Lett.* **98** 013112
[40] Shao L, Ruther M, Linden S, Wegener M and Weissmüller J 2012 On the mechanism of electrochemical modulation of plasmonic resonances *Appl. Phys. Lett.* **101** 121109
[41] Klein M W, Enkrich C, Wegener M and Linden S 2006 Second-harmonic generation from magnetic metamaterials *Science* **313** 502
[42] Klein M W, Wegener M, Feth N and Linden S 2007 Experiments on second- and third-harmonic generation from magnetic metamaterials *Opt. Express* **15** 5238
[43] Feth N *et al* 2008 Second-harmonic generation from complementary split-ring resonators *Opt. Lett.* **33** 1975
[44] Linden S, Niesler F B P, Förstner J, Grynko Y, Meier T and Wegener M 2012 Collective effects in second-harmonic generation from split-ring-resonator arrays *Phys. Rev. Lett.* **109** 015502
[45] Luo L, Chatzakis I, Wang J, Niesler F B P, Wegener M, Koschny T and Soukoulis C M 2014 Broadband terahertz generation from metamaterials *Nat. Commun.* **5** 3055
[46] Niesler F B P, Feth N, Linden S, Niegemann J, Gieseler J, Busch K and Wegener M 2009 Second-harmonic generation from split-ring resonators on a GaAs substrate *Opt. Lett.* **34** 1997
[47] Meinzer N, Ruther M, Linden S, Soukoulis C M, Khitrova G, Hendrickson J, Olitzky J D, Gibbs H M and Wegener M 2010 Arrays of Ag split-ring resonators coupled to InGaAs single-quantum-well gain *Opt. Express* **18** 24140
[48] Meinzer N, König M, Ruther M, Linden S, Khitrova G, Gibbs H M, Busch K and Wegener M 2011 Distance-dependence of the coupling between split-ring resonators and single-quantum-well gain *Appl. Phys. Lett.* **99** 111104
[49] Wegener M, Garcia Pomar J L, Soukoulis C M, Meinzer N, Ruther M and Linden S 2008 Toy model for plasmonic metamaterial resonances coupled to two-level system gain *Opt. Express* **16** 19785
[50] Fang A, Koschny T, Wegener M and Soukoulis C M 2009 Self-consistent calculation of metamaterials with gain *Phys. Rev.* B **79** 241104(R)
[51] Fang A, Huang Z, Koschny T and Soukoulis C M 2011 Overcoming losses of a split ring resonator array with gain *Opt. Express* **19** 12688
[52] Fang A, Koschny T and Soukoulis C M 2010 Self-consistent calculations of loss compensated fishnet metamaterials *Phys. Rev.* B **82** 121102(R)
[53] Fang A, Koschny T and Soukoulis C M 2010 Lasing in metamaterials nanostructures *J. Opt.* **12** 024013
[54] Huang Z, Koschny T and Soukoulis C M 2012 Theory of pump-probe experiments of metallic metamaterials coupled to the gain medium *Phys. Rev. Lett.* **108** 187402
[55] Droulias S, Fietz C, Zhang P, Koschny T and Soukoulis C M 2014 Lasing threshold control in 2D photonic crystals with gain *Opt. Express* **22** 19242
Droulias S, Jain A, Koschny T and Soukoulis C M 2017 Novel lasers based on resonant dark states *Phys. Rev. Lett.* **118** 073901
[56] Huang Z, Droulias S, Koschny T and Soukoulis C M 2014 Mechanism of the metallic metamaterials coupled to the gain material *Opt. Express* **22** 28596
[57] Tassin P, Koschny T and Soukoulis C M 2013 Graphene for terahertz applications *Science* **341** 620
[58] Shen N, Tassin P, Koschny T and Soukoulis C M 2014 Comparison of gold- and graphene-based resonant nanostructures for THz metamaterials and an ultrathin graphene-based modulator *Phys. Rev.* B **90** 115437
[59] Tassin P, Koschny T, Kafesaki M and Soukoulis C M 2012 A comparison of graphene, superconductors and metals as conductors for metamaterials and plasmonics *Nat. Photon.* **6** 259
[60] Decker M, Klein M W, Wegener M and Linden S 2007 Circular dichroism of planar chiral magnetic metamaterials *Opt. Lett.* **32** 856
[61] Decker M, Ruther M, Kriegler C, Zhou J, Soukoulis C M, Linden S and Wegener M 2009 Strong optical activity from twisted-cross photonic metamaterials *Opt. Lett.* **34** 2501
[62] Decker M, Zhao R, Soukoulis C M, Linden S and Wegener M 2010 Twisted split-ring-resonator photonic metamaterial with huge optical activity *Opt. Lett.* **35** 1593
[63] Gansel J K, Thiel M, Rill M S, Decker M, Bade K, Saile V, von Freymann G, Linden S and Wegener M 2009 Gold helix photonic metamaterial as broadband circular polarizer *Science* **325** 1513
[64] Gansel J K, Wegener M, Burger S and Linden S 2010 Gold helix photonic metamaterials: a numerical parameter study *Opt. Express* **18** 1059
[65] Gansel J K, Latzel M, Frölich A, Kaschke J, Thiel M and Wegener M 2012 Tapered-gold-helix metamaterials as improved circular polarizers *Appl. Phys. Lett.* **100** 101109
[66] Kaschke J, Gansel J K and Wegener M 2012 On metamaterial circular polarizers based on metal N-helices *Opt. Express* **20** 26012
[67] Kaschke J, Blome M, Burger S and Wegener M 2014 N-helical metamaterials with three-fold rotational symmetry *Opt. Express* **22** 19936
[68] Fischer J and Wegener M 2013 Three-dimensional optical laser lithography beyond the diffraction limit *Laser Photon. Rev.* **7** 22
[69] Kaschke J and Wegener M 2015 Gold triple-helix mid-infrared metamaterial by STED-inspired laser lithography *Opt. Lett.* **40** 3986
[70] Kaschke J and Wegener M 2016 Optical and infrared helical metamaterials *Nanophotonics* **5** 38
[71] Kaschke J, Blume L, Wu L, Thiel M, Bade K, Yang Z and Wegener M 2015 A helical metamaterial for broadband circular polarization conversion *Adv. Opt. Mater.* **3** 3411
[72] Schmied R, Halimeh J C and Wegener M 2010 Conformal carpet and grating cloaks *Opt. Express* **18** 24361
[73] Halimeh J C, Schmied R and Wegener M 2011 Newtonian photorealistic ray tracing of grating cloaks and correlation-function-based cloaking-quality assessment *Opt. Express* **19** 6078

[74] Halimeh J C and Wegener M 2012 Time-of-flight imaging of invisibility cloaks *Opt. Express* **20** 63
[75] Halimeh J C and Wegener M 2012 Photorealistic ray tracing of free-space invisibility cloaks made of uniaxial dielectrics *Opt. Express* **20** 28330
[76] Halimeh J C and Wegener M 2013 Photorealistic rendering of unidirectional free-space invisibility cloaks *Opt. Express* **21** 9457
[77] Ergin T, Stenger N, Brenner P, Pendry J B and Wegener M 2010 Three-dimensional invisibility cloak at optical wavelengths *Science* **328** 337
[78] Fischer J, Ergin T and Wegener M 2011 Three-dimensional polarization-independent visible-frequency carpet invisibility cloak *Opt. Lett.* **36** 2059
[79] Ergin T, Fischer J and Wegener M 2011 Optical phase cloaking of 700 nm light waves in the far field by a three-dimensional carpet cloak *Phys. Rev. Lett.* **107** 173901
[80] Halimeh J C, Thompson R T and Wegener M 2016 Invisibility cloaks in relativistic motion *Phys. Rev.* A **93** 013850
[81] Schumann M F, Wiesendanger S, Goldschmidt J C, Bläsi B, Bittkau K, Paetzold U W, Sprafke A, Wehrspohn R, Rockstuhl C and Wegener M 2015 Cloaked contact grids on solar cells by coordinate transformations: designs and prototypes *Optica* **2** 850
[82] Schittny R, Kadic M, Bückmann T and Wegener M 2014 Invisibility cloaking in a diffusive light scattering medium *Science* **345** 427
[83] Schittny R, Niemeyer A, Kadic M, Bückmann T, Naber A and Wegener M 2015 Transient behavior of invisibility cloaks for diffusive light propagation *Optica* **2** 84
[84] Schittny R, Niemeyer A, Kadic M, Bückmann T, Naber A and Wegener M 2015 Diffuse-light all-solid-state invisibility cloak *Opt. Lett.* **40** 4202
[85] Schittny R, Niemeyer A, Mayer F, Naber A, Kadic M and Wegener M 2016 Invisibility cloaking in light scattering media *Laser Photon. Rev.* **10** 382
[86] Mayer F, Schittny R, Egel A, Niemeyer A, Preinfalk J, Lemmer U and Wegener M 2016 Cloaking contacts on large-area organic light-emitting diodes *Adv. Opt. Mater.* **4** 740
[87] Schittny R, Kadic M, Guenneau S and Wegener M 2013 Experiments on transformation thermodynamics: molding the flow of heat *Phys. Rev. Lett.* **110** 195901
[88] Stenger N, Wilhelm M and Wegener M 2012 Experiments on elastic cloaking in thin plates *Phys. Rev. Lett.* **108** 014301
[89] Kadic M, Bückmann T, Stenger N, Thiel M and Wegener M 2012 On the practicability of pentamode mechanical metamaterials *Appl. Phys. Lett.* **100** 191901
[90] Schittny R, Bückmann T, Kadic M and Wegener M 2013 Elastic measurements on macroscopic 3D pentamode metamaterials *Appl. Phys. Lett.* **103** 231905
[91] Kadic M, Bückmann T, Schittny R, Gumbsch P and Wegener M 2014 Pentamode metamaterials with independently tailored bulk modulus and mass density *Phys. Rev. Appl.* **2** 054007
[92] Bückmann T, Thiel M, Kadic M, Schittny R and Wegener M 2014 An elasto-mechanical unfeelability cloak made of pentamode metamaterials *Nat. Commun.* **5** 4130
[93] Bückmann T, Kadic M, Schittny R and Wegener M 2015 Cloak design by direct lattice transformation *Proc. Natl Acad. Sci. USA* **112** 4930
[94] Kadic M, Bückmann T, Schittny R and Wegener M 2013 Metamaterials beyond electromagnetism *Rep. Prog. Phys.* **76** 126501
[95] Bückmann T, Kadic M, Schittny R and Wegener M 2015 Mechanical metamaterials with anisotropic effective mass density tensor made from one constituent *Phys. Status Solidi* b **7** 1671
[96] Qu J, Kadic M, Naber A and Wegener M 2017 3D micro-printed two-component metamaterials with negative thermal-expansion coefficient from positive constituents *Sci. Rep.* **7** 40643
[97] Frenzel T, Findeisen C, Kadic M, Gumbsch P and Wegener M 2016 Tailored buckling micro-lattices as reusable light-weight shock absorbers *Adv. Mater.* **28** 5865
[98] Kadic M, Schittny R, Bückmann T, Kern C and Wegener M 2015 Hall-effect sign-inversion in a realizable 3D metamaterial *Phys. Rev.* X **5** 021030
[99] Kern C, Kadic M and Wegener M 2015 Parallel Hall Effect from three-dimensional single-component metamaterials *Appl. Phys. Lett.* **107** 132103
[100] Kern C, Kadic M and Wegener M 2017 Experimental evidence for sign reversal of the Hall coefficient in three-dimensional metamaterials *Phys. Rev. Lett.* **118** 016601
[101] Soukoulis C M 2006 Bending back light: the science of negative index materials *Opt. Photon. News* **17** 16
[102] Soukoulis C M, Kafesaki M and Economou E N 2006 Negative index materials: new frontiers in optics *Adv. Mater.* **18** 1941
[103] Soukoulis C M, Linden S and Wegener M 2007 Negative refractive index at optical wavelengths *Science* **315** 47
[104] Soukoulis C M and Wegener M 2011 Past achievements and future challenges in the development of three-dimensional photonic metamaterials *Nat. Photon.* **5** 523
[105] Soukoulis C M and Wegener M 2010 Optical metamaterials: more bulky and less lossy *Science* **330** 1633
[106] Wegener M 2013 Metamaterials beyond optics *Science* **342** 939
[107] Christensen J, Kadic M, Kraft O and Wegener M 2015 Vibrant times for mechanical metamaterials *MRS Commun.* **5** 453